Single camera time-resolved 3D tomographic reconstruction of a pulsed gas jet

J. M. Cabaleiro, J. L. Aider, G. Artana & J. E. Wesfreid

Journal of Visualization

ISSN 1343-8875

J Vis
DOI 10.1007/s12650-013-0176-z

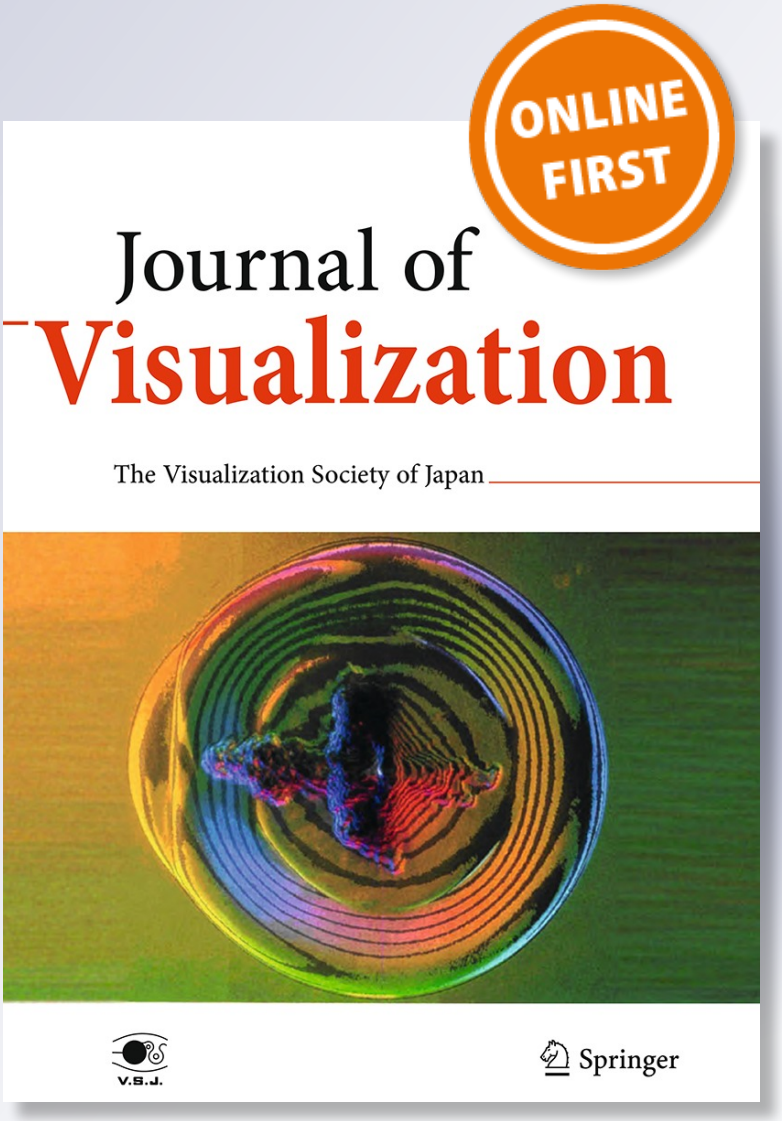

Springer

Your article is protected by copyright and all rights are held exclusively by The Visualization Society of Japan. This e-offprint is for personal use only and shall not be self-archived in electronic repositories. If you wish to self-archive your article, please use the accepted manuscript version for posting on your own website. You may further deposit the accepted manuscript version in any repository, provided it is only made publicly available 12 months after official publication or later and provided acknowledgement is given to the original source of publication and a link is inserted to the published article on Springer's website. The link must be accompanied by the following text: "The final publication is available at link.springer.com".

Author's personal copy

J Vis
DOI 10.1007/s12650-013-0176-z

REGULAR PAPER

J. M. Cabaleiro · J. L. Aider · G. Artana · J. E. Wesfreid

Single camera time-resolved 3D tomographic reconstruction of a pulsed gas jet

Received: 12 October 2012 / Revised: 12 March 2013 / Accepted: 11 May 2013
© The Visualization Society of Japan 2013

Abstract Experimental characterization of micro-jets is challenging because of the small dimensions of the micro-nozzle. In this study, we propose a new technique to visualize the instantaneous 3D structure of a pulsed gas micro-jet. Using phase-averaging of Schlieren visualizations obtained with a high-speed camera and 3D reconstruction through a filtered back projection algorithm, it is possible to follow the high-speed dynamics of the pulsed jet. The experimental technique is illustrated by a 3D reconstruction of a pulsed helium micro-jet. The technique is simple yet very useful. To our knowledge, it is the only experimental method to analyze the instantaneous 3D structure and high frequency dynamics of pulsed micro-jets.

Keywords Tomographic reconstruction · Micro-jet · Schlieren

1 Introduction

Continuous or pulsed micro-jets are now used in many academic or industrial applications like flow control (Aubrun et al. 2011; Joseph et al. 2012), noise reduction (Castelain et al. 2008), CPU cooling, or even micro-thrusters (Moríñigo and Quesada 2008). Despite being more and more commonly used, the properties of micro-jets are not well known and it is not clear whether the transitions and phenomena encountered on large-scale jets can be recovered at small scales (Gau et al. 2009).

Indeed, because of the very small dimensions of their micro-nozzles, it is very difficult to measure jet velocity profiles. For micro-nozzle diameters or widths (for rectangular cross-sections) smaller than 0.5 mm, it becomes impossible to use most of the classic experimental techniques. Hot-wire measurement is intrusive and the length of the wire is too long to be used close to micro-nozzle outlet. Particle image velocimetry measurements require oil micro-droplets seeding which stick to the wall inside the micro-channels and micro-nozzle. It is then important to find an experimental technique that is non-intrusive and does not

J. M. Cabaleiro · G. Artana
CONICET-Fluid Dynamics Laboratory, Faculty of Engineering,
University of Buenos Aires, Buenos Aires, Argentina

J. M. Cabaleiro (✉)
Microfluidics and Plasma Laboratory, Marina Mercante University,
Buenos Aires, Argentina
E-mail: jmcabaleiro@fi.uba.ar
Tel.: +5411-4343-0092
Fax: +5411-4343-0092

J. L. Aider · J. E. Wesfreid
Laboratoire PMMH, UMR 7636 CNRS, UPMC, UPD, ESPCI ParisTech,
10 rue Vauquelin, 75231 Paris, France

Published online: 08 September 2013

Author's personal copy

require seeding. Molecular tagging velocimetry is an interesting solution (Lempert et al. 2003; Fermigier et al. 1980): it does not require any seeding and is non-intrusive. It is nevertheless difficult to use at small scales with a complex optical setup and is expensive (two different lasers for tagging and visualizing). Optical methods based on variations of the refractive index appear as well-suited techniques for micro-jets. In subsonic flows, however, those methods require either using a different gas or heated air for the refractive index variations to exist.

Optical methods relying on refractive index variations have been used to study gas flows for decades (Settles 2001; Vasiliev 1971; Goldstein 1996; Tropea et al. 2007). Mainly qualitative results are generally obtained with these methods. Interferometric methods provide information on the refractive index of the medium, whereas Schlieren methods provide information on its first derivative and Shadowgraph methods on its second derivative. In this work we focus on Schlieren methods.

The refractive index of a gas can be considered proportional to the local density, following the Gladstone-Dale law. Therefore, depending on the experiment and the procedure used, one can obtain the density field from Schlieren images. The information provided in a Schlieren image is "line-of-sight (l-o-s) integrated". That is, the contrast in the image is proportional to the l-o-s integration of the first spatial derivative of the refractive index perpendicular to the knife-edge (Fig. 4). The proportionality constant is related to the optics (focal distance of the second mirror in our setup), and to the amount of light stopped by the knife-edge.

If the flow under study is two-dimensional or axisymmetric, a single image suffices to obtain the instantaneous refractive index field (and thus, the density field). On the other hand, if the flow is not axisymmetric and the gradient of the density field changes along the integration line (as it occurs in many three-dimensional flows), multiple projections are necessary to obtain the refractive index field. The number of necessary projections increases with the complexity of the flow. The method used to reconstruct the refractive index field is based on tomography. The tomographic data acquisition is conventionally modeled by the Radon transform (Radon 1917), which collects line integrals across the medium at different angles.

Mainly two methods are used in tomographic reconstruction: the algebraic reconstruction technique and the filtered back projection (FBP) algorithm (Kak and Slaney 1988). The first one is an iterative method, which is generally preferred when the number of projections is too low. The major disadvantage of this method is that it is time consuming, and that the errors may increase after a certain number of iterations, while FBP is faster and accurate, as long as the number of projections is high enough (Feng et al. 2002).

There are several studies regarding 3D density measurements that combine Schlieren or interferometric techniques with tomographic reconstruction. Dalziel et al. (2000) measured wave amplitudes generated by an oscillating cylinder using "Synthetic Schlieren". Timmerman and Watt (1995) developed a dual-reference beam, plane-wave illumination, holographic interferometry setup that provided six simultaneous views of a compressible flow field for its reconstruction. Feng et al. (2002) used a Mach–Zehnder holographic interferometer and FBP to study a stationary non-axisymmetric flow of a helium-air mixture. Venkatakrishnan and Meier (2004) used background oriented schlieren (BOS) to obtain l-o-s integrated density gradients of a stationary cone-cylinder flow (with rotational symmetry) at Mach 2. They derived those l-o-s integrated density gradients and later integrated the resulting Poisson equation. The result was a l-o-s integrated density field, which was then back projected to a density field slice using FBP. Later Venkatakrishnan and Suriyanarayanan (2009) used BOS data to study the supersonic flow past an afterbody, assuming axisymmetry for the 3D reconstruction. Goldhahn and Seume (2007) and Goldhahn et al. (2009) also used BOS and FBP to study an under-expanded free jet of air and also the wake of a cascade wind tunnel. Their procedure uses the BOS gradient data directly to reconstruct the 3D field. Masanori et al. (2011) used colored-grid BOS (CGBOS) and laser interferometric computed tomography to study stationary supersonic flow around an asymmetric body. Finally, Atcheson et al. (2008) used BOS and a novel tomographic algorithm to study non-stationary gas flows, but they used as much as 16 cameras simultaneously.

In this paper, we present a simple experimental method to obtain 3D reconstructions of non-stationary, non-axisymmetric pulsed jet flows, using a classic Schlieren setup and one high-speed camera. In the next section, the experimental setup and the algorithm used for the 3D reconstruction are presented. In the third section, the results are presented. In the fourth section, different FBP filters are compared, and the density fields are calculated. Finally, a time evolution of the 3D structure of the micro-jet is illustrated before coming to the conclusion.

Author's personal copy

2 Experimental setup

2.1 The micro-jet

The pulsed micro-jet setup is shown in Fig. 1. Helium is fed to the micro-nozzle at a given upstream pressure. One can see guiding vanes inside the micro-nozzle, which correspond to the design of micro-nozzles of MEMS actuators used for flow control experiments (Joseph et al. 2012, 2013). The micro-nozzle cross-section is 0.38 mm thick (the "micro" dimension) and 12.5 mm long. The design of the micro-nozzle is associated with the micro-fabrication process: MEMS pulsed micro-jets are drilled into SOI wafers and therefore always have a planar geometry where the depth is limited by the thickness of the SOI wafer. Even if the nozzle geometry can be seen as 2D, the flows obtained in this work are fully 3D, as it will be shown in the next sections. The jet pulse frequency F_j is set by means of a fast solenoid valve (Matrix Mechatronics, Model 821) and ranges between 0 and 500 Hz.

2.2 The Schlieren setup

The setup consists of a traditional z-type Schlieren system (Fig. 2): two spherical mirrors (diameter: 0.15 m, focal distance: 1.50 m, Edmund Optics) are placed on the corners of an antivibration optical table. An AI high intensity coaxial LED spot light illuminator (Edmund Optics) with a condenser is placed on one side of the centerline, at the focal distance of the first mirror. On the other side, a vertical knife-edge (the edge is parallel to z-axis) is placed at the focal distance of the second mirror, and after that, a high-speed camera (Photron FASTCAM SA4) and lens (Nikon 70–300 mm f/4.5–5.6 G AF-S VR NIKKOR).

Both the light source and the knife-edge must be located as close to the centerline as possible to minimize coma and astigmatism (Settles 2001). In our setup, the angle α between light rays was less than 6° (Fig. 3). The test section is located at the middle of the centerline. In that region we placed the micro-jet. The particularity of our experiment is to allow the micro-nozzle to turn around its vertical axis as indicated by the arrow in Figs. 3 and 4.

The high-speed camera can record 1 Mpixels pictures at $F_{ac} = 3.5$ kHz. The acquisition frequency F_{ac} can be increased up to 500 kHz by decreasing the region of interest of the sensor to 128 pixels by 16 pixels.

As shown in Figs. 2 and 3, two sets of coordinates are used.

2.3 The Radon transform and filtered back projection

As it was introduced earlier, the aim of this work is to perform a tomographic reconstruction of a micro-jet. In this section, we present the mathematical basis of the algorithm used for that reconstruction, which is a FBP. The tomographic data acquisition can be modeled by the Radon transform (Radon 1917), which collects line integrals across the medium at different angles. Given a certain function $f(x,y)$, its Radon transform is:

$$P_\theta(s) = \int_{-\infty}^{+\infty}\int_{-\infty}^{+\infty} f(x,y)\delta(x\cos\theta + y\sin\theta - s)\mathrm{d}x\mathrm{d}y = \int_{(\theta,s)\text{line}} f(x,y)\mathrm{d}l \tag{1}$$

where δ is the Dirac delta function. The coordinate systems used are shown in Fig. 4.

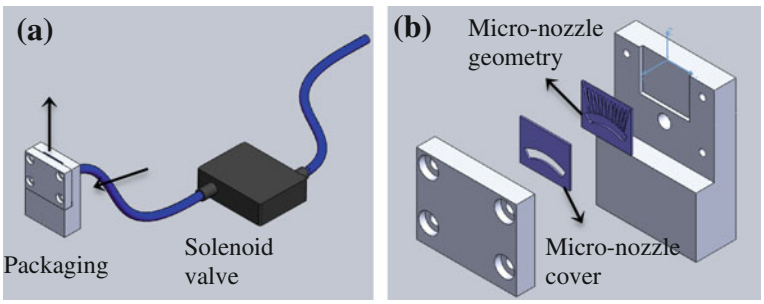

Fig. 1 **a** Packaging and solenoid valve assembly. **b** Micro-nozzle geometry and packaging

Author's personal copy

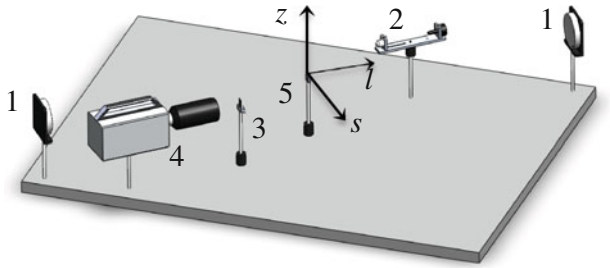

Fig. 2 Experimental setup: *1* spherical mirrors. *2* Light source. *3* Vertical knife-edge. *4* Camera and lens. *5* Micro-nozzle

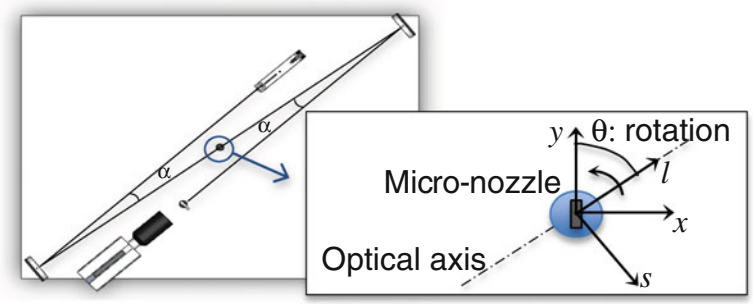

Fig. 3 Optical path: z-type Schlieren setup. The angles $\alpha < 6^{\circ}$ are small enough to minimize the coma and astigmatism. The micro-nozzle can rotate (angle θ) around the jet axis perpendicular to the horizontal plane. The micro-jet coordinates system (x, y, z) is defined

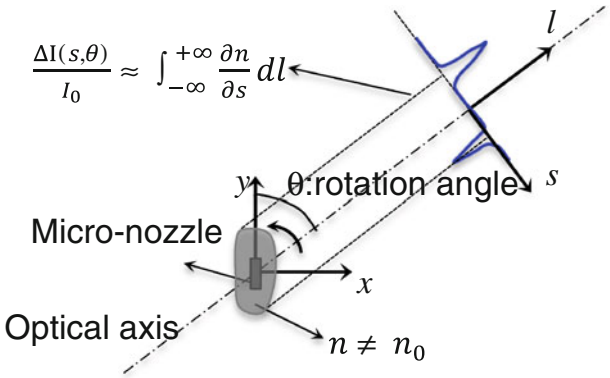

Fig. 4 Sketch of a Schlieren measurement of the micro-jet whose longer axis is rotated a given θ from the optical axis

By the use of the Fourier slice theorem we know that the Fourier transform of a projection $P(s)$ for a given θ represents the two-dimensional Fourier transform at a spatial frequency of ($u = w \cos\theta$, $v = w \sin\theta$):

$$S_\theta(w) = \int_{-\infty}^{+\infty} P_\theta(s) e^{-j2\pi ws} \mathrm{d}s = F(w,\theta) = F(w\ \cos\theta, w\ \sin\theta) \tag{2}$$

which is the two-dimensional Fourier transform on radial lines at an angle θ. If a projection were obtained for every angle θ, the inverse two-dimensional Fourier transform would give the function $f(x,y)$. Using the property:

$$F(w,\theta+\pi) = F(-w,\theta) \tag{3}$$

Author's personal copy

The inverse two-dimensional Fourier transform may be written as:

$$f(x,y) = \int_0^{\pi} \left[\int_{-\infty}^{+\infty} S_\theta(w)|w| e^{j2\pi ws} \mathrm{d}w \right] \mathrm{d}\theta \tag{4}$$

The term between brackets in Eq. (4) represents a filtering operation with a frequency response of the filter given by $|w|$. Thus, it is called a "filtered projection". Equation (4) calls for the back projection of those filtered projections.

2.4 Application to Schlieren images

In our setup, the reconstruction consists of several steps. The first one is to calculate phase-locked image averages over 20 cycles for each projection direction. Then we subtract the image background (without the jet). We are interested in reconstructing the jet morphology and to do that, we need information on the refractive index n. However, in the images we obtain (with a vertical knife-edge) the intensity I is proportional to the l-o-s integrated refractive index horizontal gradient (Figs. 5, 6, 7):

$$\Delta I = \frac{f_2}{a_\mathrm{k}} I_0 \int_{-\infty}^{+\infty} \frac{\partial n}{\partial s} \mathrm{d}l \tag{5}$$

where I is the intensity and I_0 is the background intensity without flow, and f_2 is the focal distance of the second mirror. For a rectangular light source, which forms an image of size $a \times b$ at the knife-edge (b being the dimension in the direction parallel to the knife-edge), a_k is the size of the portion of that image unstopped by the knife-edge in the direction perpendicular to the knife-edge.

Therefore, we need to integrate ΔI levels along the horizontal direction s to obtain the l-o-s integrated refractive index difference, for a given projection angle θ:

$$\int_{s_0}^{s} \Delta I \mathrm{d}s = c_2 \int_{-\infty}^{+\infty} \int_{s_0}^{s} \frac{\partial n}{\partial s} \mathrm{d}s \, \mathrm{d}l = c_2 \int_{-\infty}^{+\infty} \left[n(s,l,z_i) - n(s_0,l,z_i) \right] \mathrm{d}l \tag{6}$$

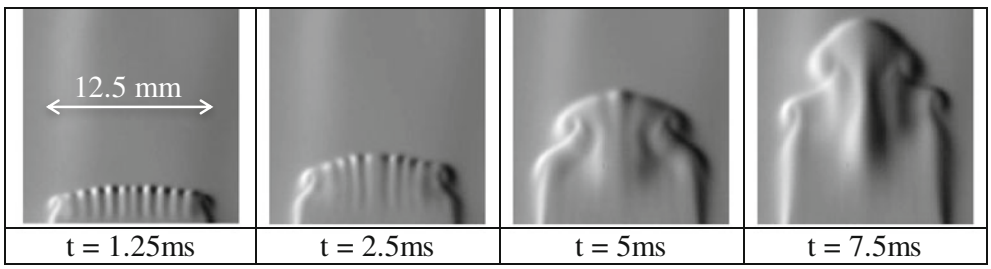

Fig. 5 Time evolution of the line-of-sight integrated refractive index horizontal gradient. Images correspond to the fixed 90° position. $P_j = 20$ mbar, $F_j = 20$ Hz, $F_\mathrm{ac} = 8$ kHz. *Image* size: 16 × 16 mm

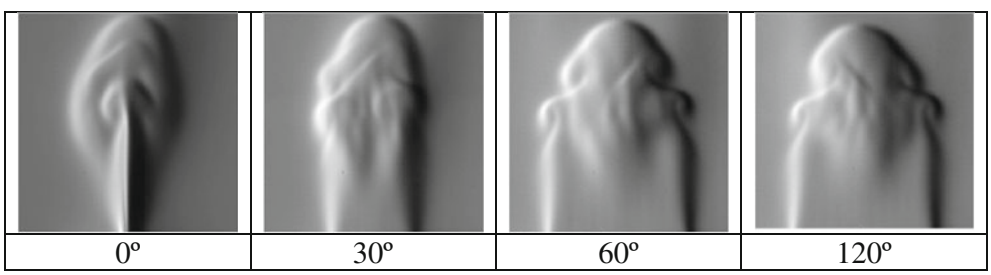

Fig. 6 Schlieren images of different views of the jet, at a fixed time ($t = 7.5$ ms) from the jet's cycle start. $P_j = 20$ mbar, $F_j = 20$ Hz, $F_\mathrm{ac} = 8$ kHz. *Image* size: 16 × 16 mm

Author's personal copy

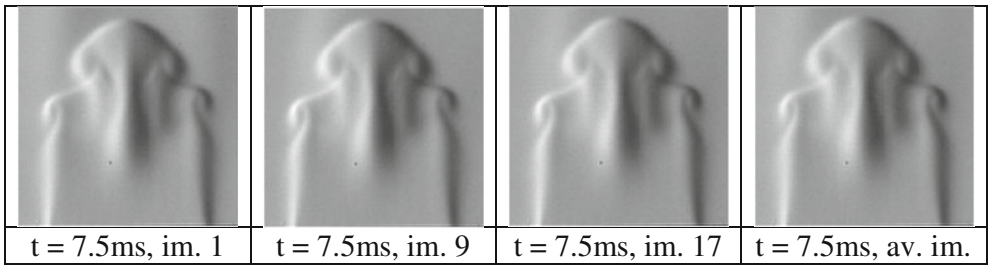

Fig. 7 Comparison between instantaneous images and average image at the same relative time

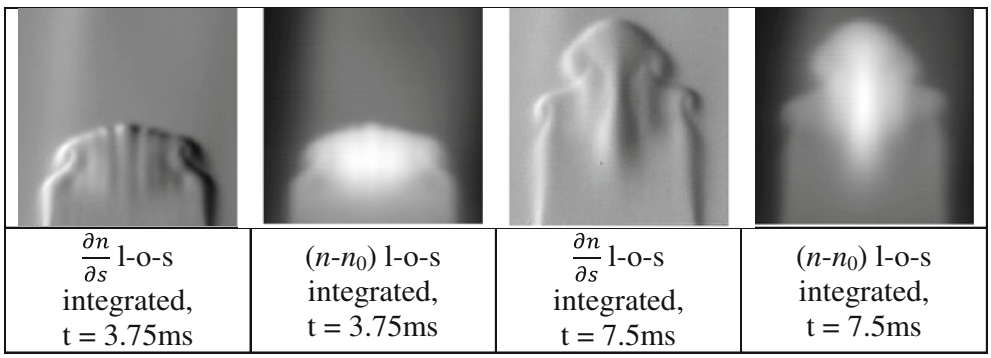

Fig. 8 Horizontal integration of Schlieren images. 90° position

If the horizontal position s_0 is far enough from the jet, we can assume that the refractive index at that position corresponds to that of the surrounding gas (n_{air}):

$$n(s_0, l, z_i) = n_{\text{air}} \tag{7}$$

After performing these integrations, the resulting images are fed to a FBP algorithm described in Kak and Slaney (1988), which essentially is the numerical implementation of the Eqs. (2) and (4), using the result of Eq. (6) as $P_\theta(s)$. For a given z_i position, the result of the FBP, $G(x, y, z_i)$, is a slice of scalar values that are proportional to the refractive index field, minus the air's (or the surrounding gas) refractive index:

$$n(x, y, z_i) - n_{\text{air}} = G(x, y, z_i)/c_2 \tag{8}$$

The value of the constant c_2 could be derived from the geometry of the setup and the background intensity level I_0, but that would require having a very good measure of the value of a_k. In our setup, $f_2 = 1.5$ m, and $a \approx 2$ mm, we set the knife-edge at 50 % so $a_k \approx 1$ mm. With this configuration, the intensity value was 68 counts (for an 8 bit image). This gives a value of $c_2 = 1.02 \times 10^5$ counts. In practice, having a good measure of a_k is quite complicated; an error of 20 % in the measurement of a_k, gives the same amount of error in c_2. Therefore we decided to estimate it considering that where G is maximum, the refractive index is that of pure helium $n_{\text{He}} = n(x, y, z_i)$. The value obtained in such a way is $c_2 = 1.18 \times 10^5$ counts, less than 20 % higher than the previous estimation.

The FBP algorithm is highly sensitive to the number of projections used. In this work, 36 projections were taken from 0° to 175°. The first position, 0°, is the position where the nozzle's exit longer dimension is aligned with the optical axis, as sketched in Fig. 4.

The algorithm uses each horizontal pixel line coming from the projections to retrieve a slice of the jet. Therefore, each slice is reconstructed from 36 horizontal lines. Then the horizontal slices obtained for every vertical position are assembled to reconstruct the 3D jet structure.

3 Results

The schlieren setup makes it possible to obtain pictures of the micro-jet like those presented in Fig. 5. In this sequence, we present the time evolution of a helium jet obtained with an upstream pressure of $P_j = 20$ mbar, at the 90° position.

Author's personal copy

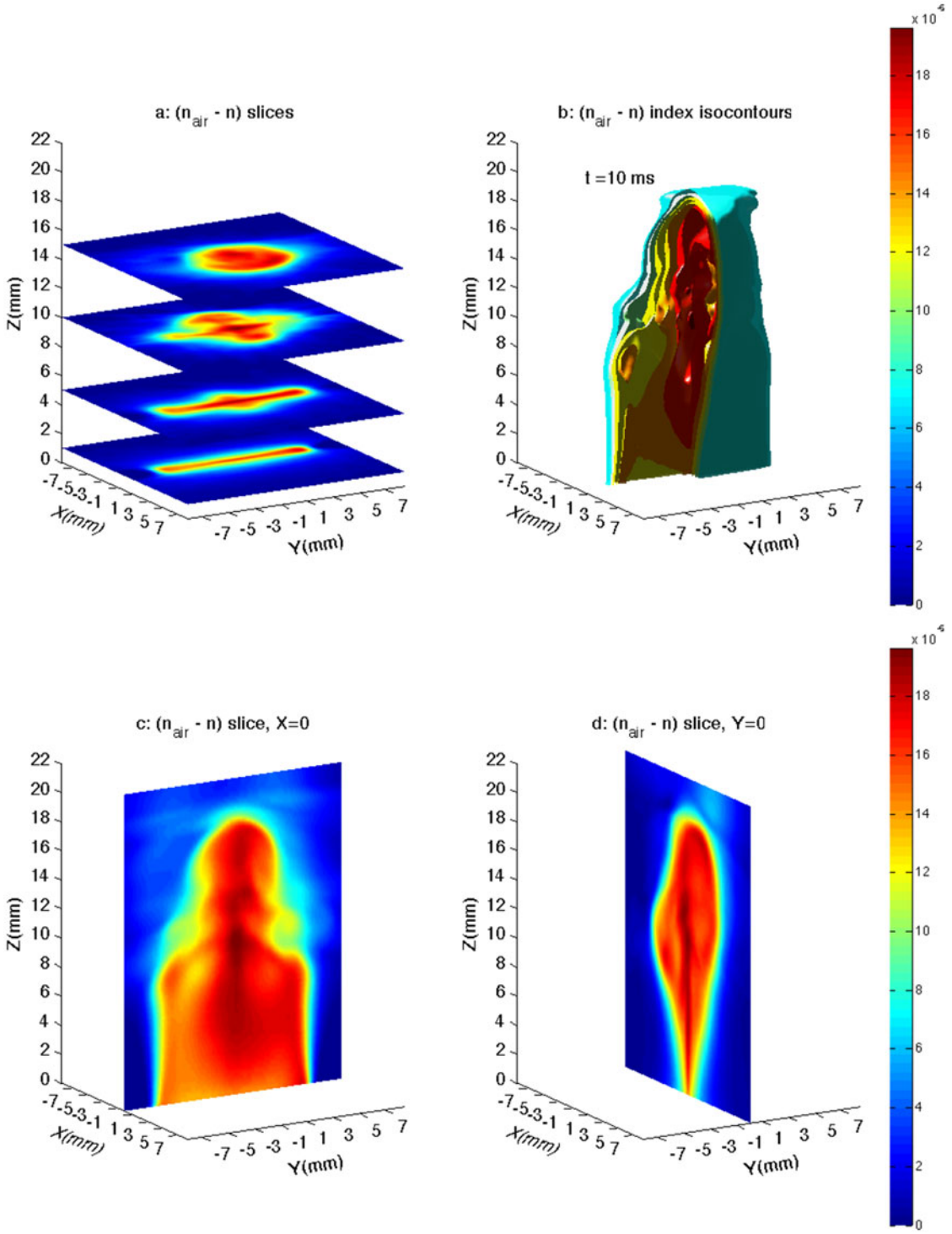

Fig. 9 **a** Horizontal slices, **b** 3D iso-contours, **c** vertical slice at $x = 0$, and **d** vertical slice at $y = 0$ of the refractive index difference. $t = 10$ ms, $P_j = 20$ mbar, $F_j = 20$ Hz

In Fig. 6, we present images obtained with the same parameters but at a fixed time from the jet start and for different angles of rotation of the micro-nozzle. The acquisition frequency was $F_{ac} = 8$ kHz for Figs. 5 and 6. The solenoid valve was set at 20 Hz for the 20 mbar jet, giving 400 images per cycle.

Author's personal copy

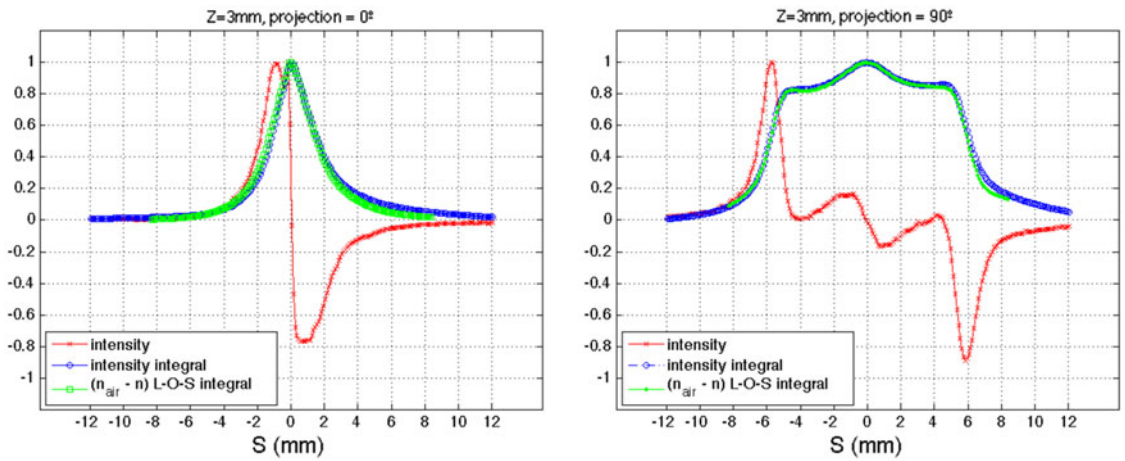

Fig. 10 Normalized Intensity levels along an image line, normalized intensity levels integral, and reconstructed (with a Hamming filter) normalized intensity levels integral. *Left*: 0° position. *Right*: 90° position. Time = 10 ms

These images are treated according to the procedure described in the previous section. This procedure is based on the fact that the observed jet is so repeatable that at the same relative time, the structures observed on different runs are the same. To confirm that, 20 cycles were observed for each projection. Figure 7 shows three random picked images of those 20 cycles at the 90° position, and the average image of the 20 cycles, showing that the repeatability observed at 20 mbar allows for this method to be applied. This was observed for every angle.

Figure 8 shows the result of Eq. (6) applied to the Schlieren images at two different times, at the 90° position.

The result of the FBP algorithm is presented in Fig. 9. Figure 9a shows the slices that are assembled together to reconstruct the 3D jet structure. A typical example is shown in Fig. 9b using refractive index iso-contours.

The instantaneous 3D structure of the micro-jet is very well recovered with a good spatial resolution (0.1 mm for each cubic voxel). To better understand the structure of the jet, two vertical slices are presented in Fig. 9c (*yz* plane) and Fig. 9d (*xz* plane).

4 Analysis

4.1 Filter comparison

Different filters are typically used in the FBP algorithm, the most mathematically rigorous one is $|w|$, as stated in Eq. (4). This filter, however, is quite sensitive to noise. In this work we have tried three different filters: Ram-Lak, Hamming, and Shepp and Logan filters (Shepp and Logan 1974; Kak and Slaney 1988; Oppenheim and Schafer 1989). To compare the FBP algorithm results using these filters, we performed a "l-o-s" integration on our reconstruction results, and compared them to the horizontally integrated intensity on the images. For the 0° projection we integrated the FBP result along y:

$$\int_{-\infty}^{+\infty} [n(x, y, z_i) - n_{\text{air}}]\, \mathrm{d}y \tag{9}$$

and for the 90° projection we integrated the FBP result along x:

$$\int_{-\infty}^{+\infty} [n(x, y, z_i) - n_{\text{air}}]\, \mathrm{d}x \tag{10}$$

The results of those integrals are presented in normalized form in Fig. 10 using a Hamming filter, together with the source image intensity, and the horizontally integrated image intensity, both also

Author's personal copy

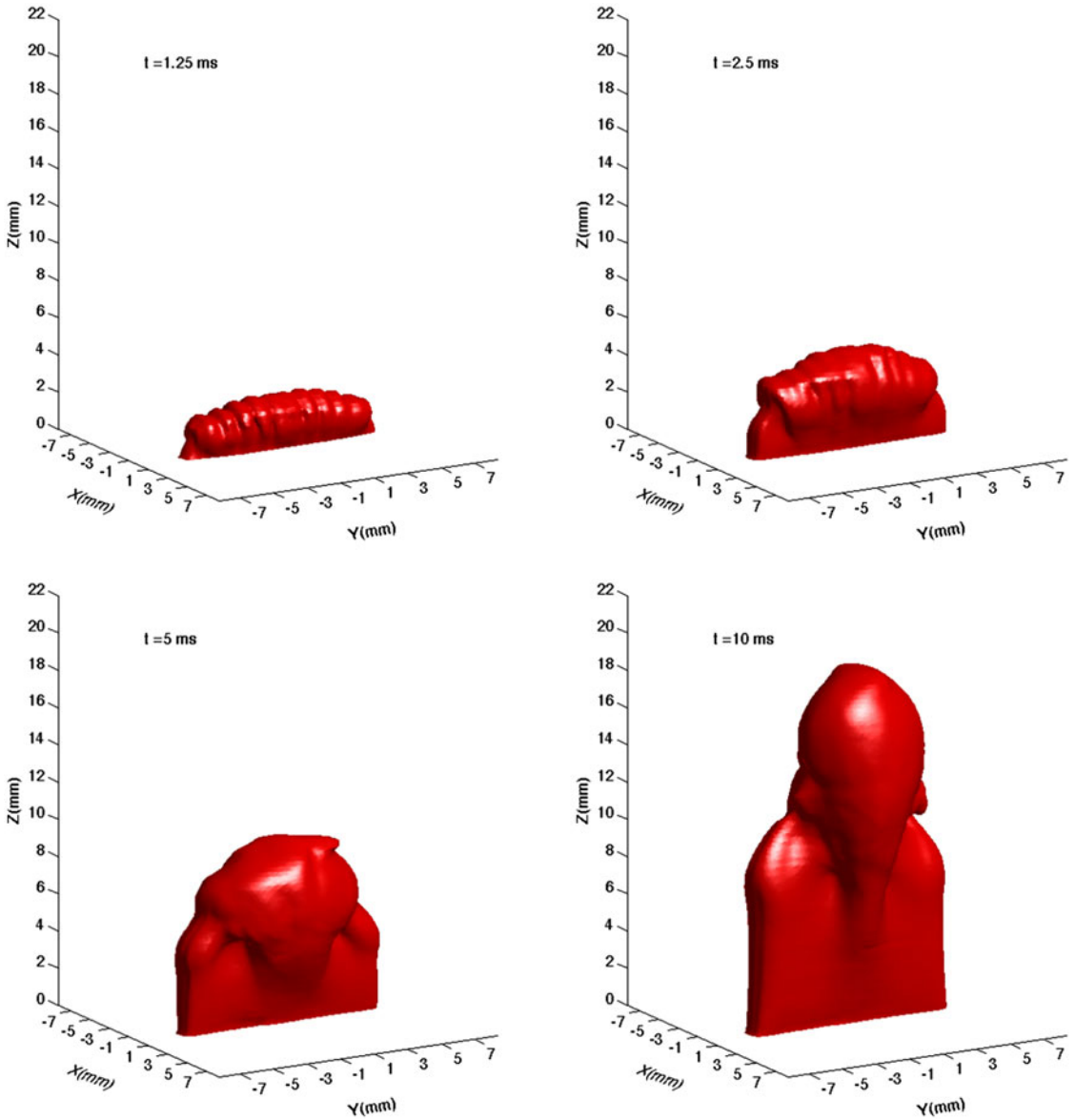

Fig. 11 3D Reconstruction at four different times. Iso-density = 0.75 kg/m^3

normalized. There is a very good agreement between the reconstruction "l-o-s" integration, and the horizontally integrated image. No significant difference was observed using the three mentioned filters for our data. All the reconstructions presented hereafter were obtained with a Hamming filter.

4.2 Density field calculation

In this work, we were mainly interested in observing and describing the structure of the transient helium micro-jet. However, it can be interesting to analyze the density field as well. If pressure and temperature are considered constant and equal for helium and air, this field can be obtained through the Gladstone-Dale equation for a helium-air mixture (Merzkirch 1974):

$$n - 1 = K_{\mathrm{He}}\rho_{\mathrm{He}} + K_{\mathrm{Air}}\rho_{\mathrm{Air}} = K_{\mathrm{He}}\chi_{\mathrm{He}}\rho_{0\mathrm{He}} + K_{\mathrm{Air}}(1 - \chi_{\mathrm{He}})\rho_{0\mathrm{Air}} \tag{11}$$

where ρ_{He} and ρ_{Air} are the partial helium and air densities. χ_{He} is the helium mole fraction. $\rho_{0\mathrm{He}}$ and $\rho_{0\mathrm{Air}}$ are pure helium and pure air densities at the laboratory conditions (20 °C and 1 atm). K_{He} and K_{Air} are the Gladstone-Dale constants for both gases, which can be found in the literature (here we used

Author's personal copy

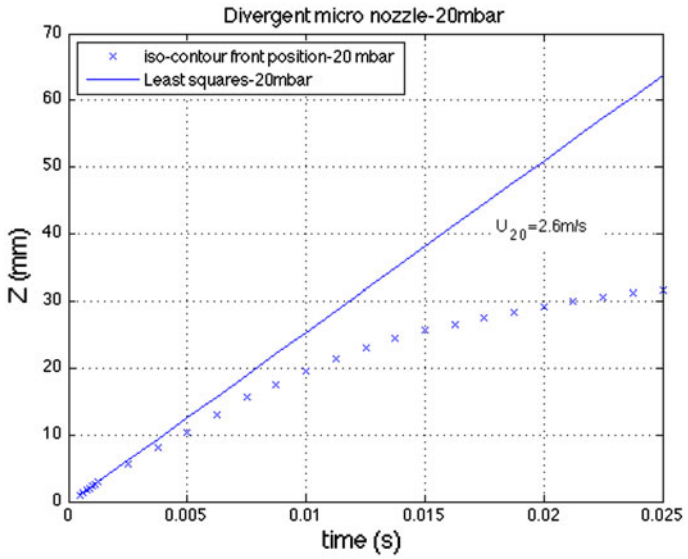

Fig. 12 Estimation of the micro-jet's front velocity. A density iso-contour is followed at the jet's axis as a function of time

$K_{He} = 1.96 \times 10^{-4}$ m^3/kg and $K_{Air} = 2.26 \times 10^{-4}$ m^3/kg). We can obtain the helium mole fraction knowing that:

$$n_{Air} - 1 = K_{Air}\rho_{0Air} \tag{12}$$

and, consequently:

$$\chi_{He} = \frac{n - n_{Air}}{(K_{He}\rho_{0He} - K_{Air}\rho_{0Air})} \tag{13}$$

Finally, once the helium mole fraction is determined throughout the volume, we obtain the density field:

$$\rho = \chi_{He}\rho_{0He} + (1 - \chi_{He})\rho_{0Air} \tag{14}$$

4.3 Time evolution of the jet structure

To show a time evolution of the 3D structure of the micro-jet, a density iso-surface level of 0.75 kg/m^3 was chosen so that it defines the "jet frontier".

Figure 11 shows such time evolution of the jet coming from our divergent nozzle with a 12.5/0.38 aspect ratio rectangular exit. Helium was fed to the nozzle at $P_j = 20$ mbar.

As shown in Fig. 1, there are several flow-guiding profiles inside the micro-nozzle that end up before the outlet of the nozzle. The traces of these guiding vanes are clearly visible on the 3D iso-surfaces on the first two time steps. The following time steps show the deformation of the front part of the micro-jet, with a bulb growing in the transverse direction. The lower part of the jet is smooth as expected for a laminar jet.

For larger time steps one can also see a transverse deformation of the iso-surface, suggesting that axis-switching (Grinstein et al. 1995; Krebs et al. 2012) may occur in these configurations. Such a phenomenon could only be witnessed properly with our experimental method. This has to be confirmed in future study.

Plotting the density iso-contour value at the jet axis against time and then calculating its temporal derivative, allowed for the calculation of the jet's front velocity. On the other hand, Schlieren image velocimetry (Arnaud et al. 2006) was performed on the images at the 90° position and the resulting velocity fields were phase-averaged (over 20 fields), finding the same values for the front velocity. Then, an estimation of the front velocity at the origin was made by a least square fit of the first five values (Fig. 12). This velocity does not necessarily coincide with the instantaneous jet velocity at the exit, and it was just used as a reference velocity. The value obtained was $u_j = 2.6$ m s^{-1}.

Author's personal copy

5 Conclusion

In this work a novel experimental method has been proposed that allows for the reconstruction of a 3D density field using classical Schlieren images taken at different rotation angles. Periodic and highly reproducible flows allow for phase-averaging of Schlieren pictures taken at different rotation angles (projections) with a single camera, one angle at the time. Using a single high-speed digital camera and a classical z-type Schlieren setup, it is possible to reconstruct a time-resolved 3D density field. Finally, the technique was applied to a pulsed micro-jet. It appears to be well suited to characterize the transitions, especially three-dimensionalization, of such high-speed micro-flows.

Acknowledgments This research has been performed with the support of the Bernardo Houssay Program (Ministerio de Ciencia, Tecnología e Innovación Productiva-CONICET, Republica Argentina; Ministère de l'enseignement supérieur et de la recherche, République Française; Ministère des affaires étrangères et européennes) and of the LIA PMF-FMF (French-Argentinian International Associated Laboratory in Physics and Fluid Mechanics) and of the French Agence pour le Développement Et la Maîtrise de l'Energie (ADEME) through the project CARAVAJE.

References

Arnaud E, Memin E, Sosa R, Artana G (2006) A fluid motion estimator for Schlieren imaging velocimetry. Lect Notes Comput Sci 3951:198–210

Atcheson B, Ihrke I, Heidrich W, Tevs A, Bradley D, Magnor M, Seidel HP (2008) Time-resolved 3D capture of non-stationary gas flows. ACM Trans Graph 27(5):132

Aubrun S, McNally J, Alvi F, Kourta A (2011) Separation flow control on a generic ground vehicle using steady microjet arrays. Exp Fluids 51(5):1177–1187. doi:10.1007/s00348-011-1132-0

Castelain T, Sunyach M, Juvé D, Béra JC (2008) Jet-noise reduction by impinging microjets: an acoustic investigation testing microjet parameters. AIAA J 46(5):1081–1087

Dalziel B, Hughes GO, Sutherland BR (2000) Whole-field density measurements by 'synthetic Schlieren'. Exp Fluids 28(4):322–335

Feng J, Okamoto K, Tsuru D, Madarame H, Fumizawa M (2002) Visualization of 3D gas density distribution using optical tomography. ChemEng J 86:243–250

Fermigier M, Guyon E, Jenffer P, Petit L (1980) A direct optical measurement of velocity gradients. Appl Phys Lett 36:361–362

Gau C, Shen CH, Wang ZB (2009) Peculiar phenomenon of micro-free-jet flow. Phys Fluids. doi:10.1063/1.3224012 (21, 092001)

Goldhahn E, Seume J (2007) The background oriented Schlieren technique: sensitivity, accuracy, resolution and application to a three-dimensional density field. Exp Fluids 43:241–249

Goldhahn E, Alhaj O, Herbst F, Seume J (2009) Quantitative measurements of three dimensional density fields using the background oriented Schlieren technique. Imaging Meas Methods: NNFM 106:135–144

Goldstein RJ (1996) Fluid mechanics measurements. Taylor & Francis, Washington

Grinstein FF, Gutmark E, Parr T (1995) Near field dynamics of subsonic free square jets. A computational and experimental study. Phys Fluids 7:1483–1497. doi:10.1063/1.868534

Joseph P, Amandolèse X, Aider JL (2012) Drag reduction on the 25° slant angle Ahmed reference body using pulsed jets. Exp Fluids 52(5):1169–1185. doi:10.1007/s00348-011-1245-5

Joseph P, Amandolèse X, Aider JL (2013) Flow control using MEMS pulsed micro-jets on the Ahmed body. Exp Fluids 54(1):1442. doi:10.1007/s00348-012-1442-x

Kak AC, Slaney M (1988) Principles of computerized tomographic imaging. IEEE Press, New York

Krebs F, Silva F, Sciamarella D, Artana G (2012) A three-dimensional study of the glottal jet. Exp Fluids 52(5):1133–1147. doi:10.1007/s00348-011-1247-3

Lempert W, Boehm M, Jiang N, Gimelshein S, Levin D (2003) Comparison of molecular tagging velocimetry data and direct simulation Monte Carlo simulations in supersonic micro jet flows. Exp Fluids 34:403–411

Merzkirch W (1974) Flow visualization. Academic Press Inc., New York

Moríñigo GH, Quesada JH (2008) Analysis of viscous heating in a micro-rocket flow and performance. J Therm Sci 17(2):116–124

Oppenheim AV, Schafer RW (1989) Discrete-time signal processing. Prentice-Hall, Englewood Cliffs

Masanori O, Kenta H, Hiroko K, Kazuo M (2011) Computed-tomographic density measurement of supersonic flow field by colored-grid background oriented Schlieren (CGBOS) technique. Meas Sci Technol 22:104011

Radon J (1917) On the determination of functions from their integrals along certain manifolds. Ber Saechsische Akad Wiss 29:262–277

Settles GS (2001) Schlieren and shadowgraph techniques: visualizing phenomena in transparent media. Springer Verlag, Berlin

Shepp LA, Logan BF (1974) The Fourier reconstruction of a head section. IEEE Trans Nucl Sci NS 21:21–43

Timmerman BH, Watt DW (1995) Tomographic high-speed digital holographic interferometry. Meas Sci Technol 6:1270–1277

Tropea C, Yarin A, Foss JF (2007) Handbook of experimental fluid mechanics. Springer-Verlag, Berlin

Vasiliev LA (1971) Schlieren methods. Israel Program for Scientific Translations, New York

Author's personal copy

Venkatakrishnan L, Meier GEA (2004) Density measurements using background oriented Schlieren technique. Exp Fluids 37:237–247

Venkatakrishnan L, Suriyanarayanan P (2009) Density field of supersonic separated flow past an afterbody nozzle using tomographic reconstruction of BOS data. Exp Fluids 47:463–473